Tunning pore filling of anodic alumina templates by accurate control of the bottom barrier layer thickness

C.T. Sousa[1], *D.C. Leitão*[2], *M.P. Proença*[1], *A.Apolinário*[1], *J. G. Correia*[3],
J. Ventura[1], *J.P. Araújo*[1*]

[1]IFIMUP and IN - Institute of Nanoscience and Nanotechnology, Department of Physics and Astronomy, Faculdade de Ciências da Universidade do Porto, Rua do Campo Alegre, 678, 4169-007, Porto, Portugal
[2]INESC-MN and IN, Rua Alves Redol 9, 1000-029 Lisboa, Portugal.
[3]ITN, Estrada Nacional N10, Apartado 21 – 2686-953 Sacavém, Portugal
[*]jearaujo@fc.up.pt

Abstract

The role of the alumina barrier layer thickness (δ_b) on the growth of Ni nanowires (NWs) in porous anodic alumina (PAA) was revealed. By varying the final anodization voltage to form dendrites at the bottom of the nanoporous structure, we are able to optimize δ_b (in the 2 – 16 nm range), allowing us to obtain a Ni pore filling percentage (f_p) of almost 100% for δ_b = 10 nm. However, deviations from this optimal δ_b-value led to a strong decrease of f_p. Moreover, an increase of the electrodeposition efficiency (*EE*) and NW homogeneity was also verified for δ_b up to 10 nm. Such increase in nominal δ_b leads to a consistent growth rate in all pores and consequently a complete and uniform nanopore filling. On the other hand, the decrease in electrodeposition efficiency visible for δ_b > 10 nm is related with hydrogen evolution and dielectric breakdown of the insulator layer due to the required high deposition voltages. Non-uniform NW growth is then visible, with the consequent decrease in f_p. The control of the pore filling and length homogeneity of the fabricated 1D metallic nanostructures, combined with the ability to adjust the pore dimensions of PAA, can bring novel approaches for the fabrication of nano-objects and thus exciting new applications.

1. Introduction

In the last years, great advances in nanoscience and nanotechnology have lead to the development of new platforms where physical properties such as size, porosity, geometry and surface functionalization can be controlled at the nanoscale. The research devoted to these fields is being pushed forward by the potential applications offered by nanostructures in several areas, ranging from optics to nanomedicine [1, 2]. In particular, high-aspect-ratio inorganic nanoparticles have aroused great interest, showing many novel potentialities. Among the different approaches for the fabrication of these nanoparticles, alumina template-based synthesis methods have received considerable attention as they present unique structural properties, namely a controllable pore diameter with an extremely narrow pore size distribution, and a highly self-ordered honeycomb lattice of nanoporous after a two-step anodization process [3, 4]. This closed-packed array of columnar hexagonal cells contains elongated nanopores normal to the underlying Al substrate and separated from the metal by an alumina oxide barrier layer. It is well documented that the porous anodic alumina (PAA) barrier layer thickness (δ_b) [Fig. 1] is proportional to the applied potential (V_{ap}) in the anodization process:

$$\delta_b = kV_{ap} \tag{1}$$

where $k \approx 1.3$ nmV^{-1} is a phenomenological constant [5]. Figure 1 illustrates the alumina barrier layer obtained after the second anodization at 40 V, showing a $\delta_b = 52$ nm. Only by removing or reducing this barrier layer, metallic nanowires (NWs) can be grown within PAA. Until now, three different electrodeposition methods have been developed aiming uniform and complete filling of the template pores: direct current (DC) [6], alternating current (AC) [7] and pulsed electrodeposition (PED) [8]. PED usually consists on the application of millisecond DC pulses with square shape. However, unlike DC, AC deposition and PED can be performed if a thin barrier layer is still present at the bottom of the pore. Therefore, as the removal of the Al substrate and of the barrier layer is not required for AC deposition and PED, pore filling becomes simple and straightforward, allowing the fabrication of NWs with length ranging from few nanometers to several micrometers [8]. Thus, combined PAA-PED can be a reliable and industrially compatible alternative method for the growth of nanostructures.

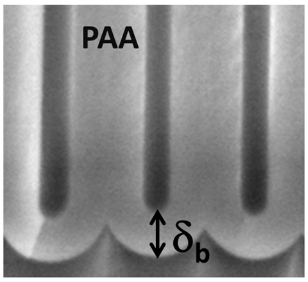

Figure 1. SEM image of the alumina barrier layer for as grown PAA ($\delta_b = 52$ nm).

To perform PED, the barrier-layer is usually thinned by a non-steady-state anodization process. An exponential decrease of the anodization potential after the second anodization [3] leads to a reproducible tree-like branched structure known as dendrites [9]. The latter results from the new anodization equilibrium state established at each step of decreasing V_{ap}, due to the combination between electrical treeing and mechanical stress. The obtained tree-like nanopores show a specific anodization current, pore density (number of pores per surface unit) and δ_b value [10].

The relatively extensive use of PAA for Ni NWs electrodeposition requires the optimization of the electrolyte, electrodeposition temperature, current density and reduction of δ_b [11 - 14]. However, few works have so far reported on the uniform growth of metallic NWs using PED [8, 14]. Moreover, there is much uncertainty concerning the optimal δ_b value to achieve an uniform filling of the alumina pores with metallic materials. The influence of δ_b is still an open issue since the chemical and structural nature of the barrier-layer is complex and ill-defined, particularly after barrier layer thinning through dendrites formation. Another important feature includes inhomogeneities in the thickness and composition of the barrier layer. Such effect is mainly related with a δ_b distribution around an average value, local defects in the Al substrate and impurities in the PAA due to the incorporation of electrolyte ions [15, 16]. More detailed studies are therefore required concerning, on the one hand, the pore structure and fluctuations in the nominal value of δ_b formed at low potential and, on the other hand, hydrogen evolution and barrier-layer dielectric-breakdown for high δ_b values [4, 15, 17]. The controlled electrodeposition of various metals inside pores is the basic step to grow arrays of multifunctional nanostructures [7, 18], and detailed studies on the particular role of δ_b could thus offer new possibilities for the improvement of branched pore filling in PAA.

In this work we were able to accurately tune δ_b by controlling the final anodization voltage. We then observed the direct influence of δ_b on the deposition behavior, since the material deposited preferably in those pores exhibiting a thinner (less resistive) barrier-layer. We provide a systematic study of the electrodeposition behavior in samples with δ_b between 2 and 16 nm, leading to the optimization of the PED conditions within PAA. Furthermore, the pore filling percentage (f_p) and the electrodeposition efficiency (EE) were analyzed to understand the influence of the barrier layer in the electrodeposition process and thus optimize δ_b. The $\%f_p$ was found to vary between 5% and 97%, and both $\%f_p$ and $\%EE$ (~78%) are maximum when $\delta_b = 10$ nm. Instead, as high deposition potentials are required for larger δ_b, non-homogeneous pore filling is achieved because competing side-reactions take place (e.g. hydrogen evolution) inhibiting the NW growth. Nevertheless, we were able to achieve a considerable inprovement in EE for optimized δ_b values, as reflected by the highly uniform filling of PAA.

2. Experimental details

PAA templates were produced by an electrochemical oxidation process in a home-made set-up. A platinum mesh was used as the cathode, while the sample (placed on top of a copper contact) worked as the anode during the anodization process. Since low temperatures reduce the possibility of local dielectric breakdown originated by the high current densities and consequent heating, the copper base was also used as cooling plate. To improve organization and reduce surface roughness, the Al surface was treated prior to the anodization process by an electropolishing optimized process in a $HClO_4$:C_2H_5OH solution (volume ratio 1: 4) at 10° C under an applied voltage of 20 V for 2 minutes [19]. To obtain nanoporous templates with large organized areas, a two step anodization process was applied [3]. The first anodization was carried out for 24 h at 2° C, in 0.3 M $(COOH)_2$ at 40 V. Afterwards, chemical dissolution of the resulting nanoporous alumina membrane was performed by submerging the sample in an aqueous solution of 0.4 M H_3PO_4 and 0.2 M H_2CrO_4 at 70° C for 12 h. The second anodization was then performed using the same conditions as the first for 4 h, leading to a 10 μm thick PAA membrane. Finally, the barrier layer is smoothly thinned by applying an exponentially decreasing voltage from 40 V down to the potential value corresponding to the desired δ_b [given by Eq. (1)] [5]. To obtain δ_b from 2 nm to 16 nm, the final voltages ranged from 1.3 to 14 V.

Ni was then electrodeposited by consecutively applying a cycle with three different pulses. Initially, the material is deposited by applying a constant current pulse (70 $mAcm^{-2}$) for 8 ms. Then, a second pulse with opposite polarity and constant potential (corresponding to the final applied potential in the anodization process) is used during 2 ms to discharge the insulator barrier layer capacitance. Finally, the cycle is closed with a rest pulse of 0.7 s where no current flows to allow the reposition of the ions in the deposition interface. The pulsed electronic signal was supplied by a SourceMetter Keithley 2400. The electrolyte used was the so-called Watts bath, composed of 1.14 M $NiSO_4.6H_2O$, 0.19M $NiCl_2.6H2O$ and 0.73M H_3BO_3. The pH value of the electrolyte was maintained at 4.0 – 5.0 and its temperature was kept constant at 40° C. The percentage of filled pores and the length of the deposited NWs were evaluated by a QUANTA-FEI high resolution scanning electron microscope (HR-SEM) using cross-section of as-deposited samples and top views after ion-milling. Cross sections were prepared by folding the samples until cracks appeared in the alumina surface. To quantitatively assess pore-filling, the as-deposited samples were milled to remove the overflown Ni in the surface in addition to 1μm of PAA template, therefore exposing the filled nanopores of the array. Milling of samples was carried out using an 1140 L ion beam sputter deposition system by Commonwealth Scientific Corporation. The f_p was determined using an open software for image analysis [20]. Finally, magnetic measurements were performed in a commercial (Quantum Design) superconducting quantum interference device (SQUID) magnetometer with an applied field up to 2 T.

3. Results and discussion

Figure 2(a) shows the potential (V_{dep}) evolution during Ni NW electrodeposition on PAA templates at constant current by PED. Different regimes can be observed in the $V_{dep}(t)$ curves [21]. First, dendrite filling occurs which is characterized by an increase in V_{dep} with time [Fig. 2(a)]. When the dendrites are fully filled, V_{dep} maximum is reached and a time (t_d) is defined. Then a quasi-constant V_{dep} behavior is visible corresponding to pore filling. Finally, when the nanowires start to emerge from the pores, a sudden decrease in V_{dep} and increase in noise is observed (not shown). The total electrodeposition time (including this last regime) to fill the PAA with 10 μm pore length was 1 h for all samples.

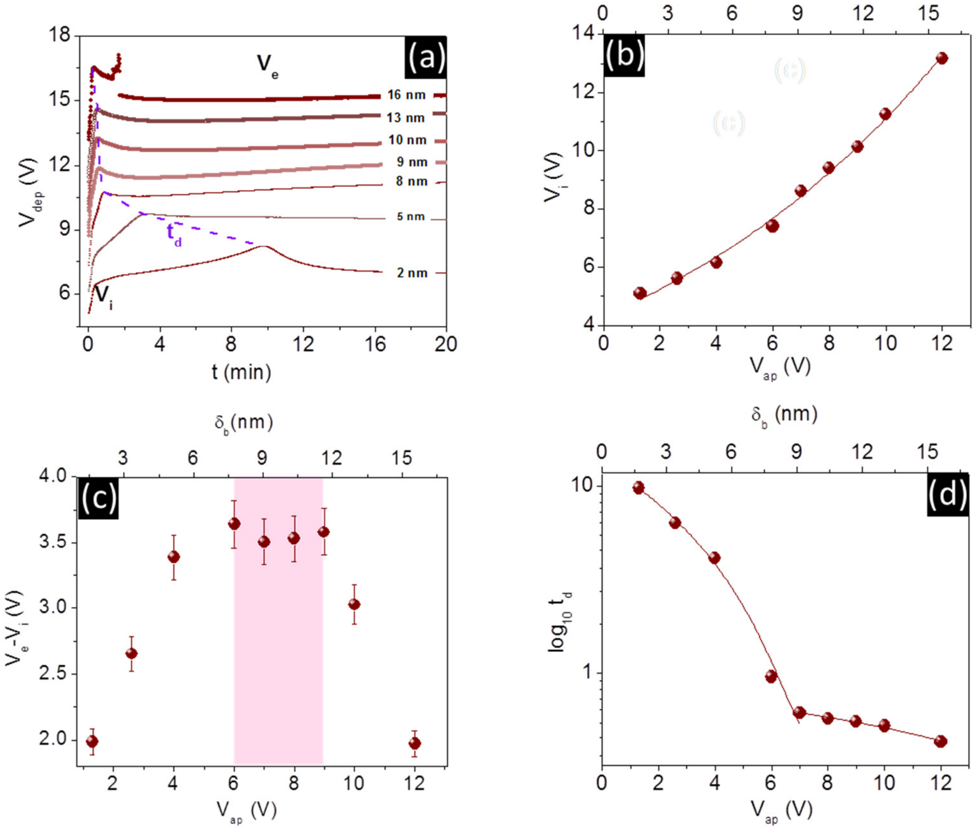

Figure 2. (a) Voltage-time curves during the filling process of PAA with Ni NWs for samples with distinct δ_b; (b) V_i vs V_{ap} and δ_b; (c) (V_e-V_i) as a function of V_{ap} and δ_b; (d) dendrites filling time vs V_{ap} and δ_b.

Another important parameter in the PED process is the initial potential (V_i) measured during the first electrodeposition pulse (8 ms), which corresponds to the deposition of the first metallic atomic layers at the pore bottom [Fig. 2(b)] [22]. Figure 2(b) also shows the fit of the V_i (δ_b) experimental data to the Simmons equation [23]:

$$V_i - V_0 = \frac{j}{J_L\sqrt{\varphi}}\delta_b e^{A\sqrt{\varphi}\delta_b} \tag{2}$$

where J_L and A are constants [23]. V_i as a function of V_{ap} (and δ_b) shows the behavior predicted by Simmons' model, indicating the presence of tunneling through the insulating oxide layer, with a potential barrier height φ = 0.13 mV and a barrier-free (δ_b= 0) potential V_0 = 4.5 V as fitting parameters. The low value obtained for φ, as compared to the ones found in the literature for alumina layers with high purity [24], is likely associated with the nature of our barrier layer which is obtained by anodization, thus presenting a fair amount of contaminating ions incorporated from the electrolyte solution. V_0 is the barrier-free voltage developed across the work and counter electrodes, including the voltage drops at the electrolyte and the work-electrode/electrolyte interface.

After the dendrites filling, V_{dep} remains almost constant during NW growth (V_e), as illustrated in Fig. 2(a). An increase of V_e with increasing V_{ap} (and δ_b) is also observed at this stage, related with the high oxide-layer resistance. Nevertheless, V_e encloses contributions arising from the external electrical contacts, the oxide layer, the electrolyte, the NWs and their interface with the electrolyte. Taking into account the geometry of our set-up and a resistivity (ρ) of the electrolyte of about 10 Ω cm [14], the estimated electrolyte resistance is ~ 13 Ω. Moreover, the estimated resistance for the barrier layer ranges from 17 Ω to 172 Ω depending on its thickness. The contributions from the external circuit, the electrolyte and the barrier layer can be eliminated subtracting V_i from V_e. In fact, $V_e - V_i$ as a function of V_{ap} [Fig. 2 (c)] can be related with NWs array growth and filling ratio, indicating an inhomogeneous growth with the majority of the NWs with a small length for $\delta_b < 7$ nm and $\delta_b > 12$ nm. However, given the metallic nature of Ni (ρ ~ 10 μΩcm), the high values of $V_e - V_i$ cannot be associated only with the NWs resistance and other complex physicochemical processes namely the increase of the electrolyte resistance should be taken into account. Further research is needed in order to clarify this point. Moreover, for low δ_b, the non-homogeneous NW growth is also corroborated by the t_d dependence on V_{ap} and δ_b [Fig. 2 (d)]. Here, t_d is defined as the local maximum in the $V_{dep}(t)$ curves [see Fig. 2(a)] and is significantly larger for low δ_b. Samples with δ_b less than 9 nm (V_{ap} 7.2 V) lead to a rapid electrodeposition into few pores, to a reduced electrodeposition rate in the neighboring ones, and consequently to higher t_d values [Fig. 2 (d)]. In contrast, the high δ_b samples yield a rapid transition between dendrite filling and the constant V_e regime.

We performed surface and cross-section SEM images for the fabricated samples (2 nm < δ_b < 16 nm). Significative differences in the growth uniformity of the Ni nanowires can be observed in Figure 3. Noticeably, for δ_b = 10 nm we observe an extremely uniform NW array, with only few empty pores located mainly at the boundary between domains of different orientations. However, even slight δ_b deviations from this optimum value lead to a rapid decrease in the NWs homogeneity and to a low number of NWs reaching the top surface.

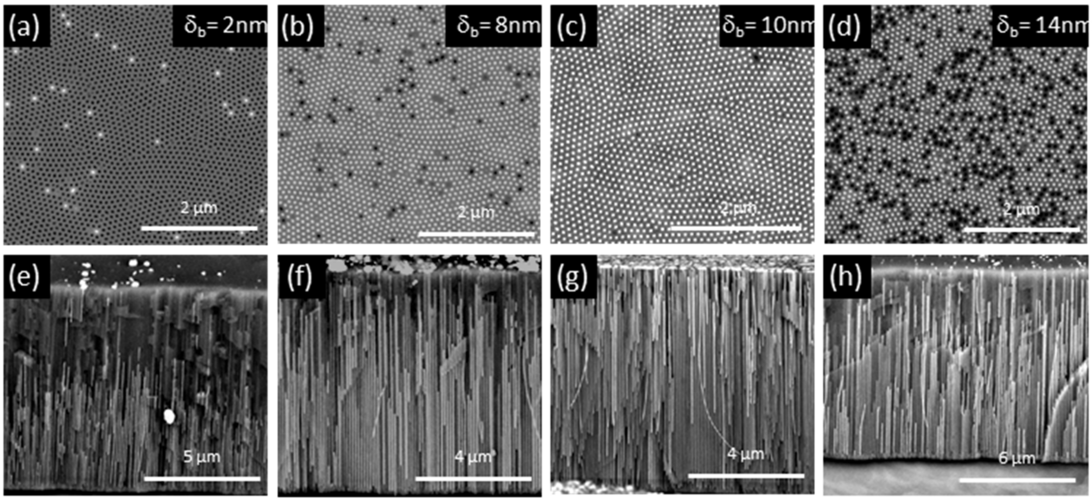

Figure 3. Influence of δ_b on the distribution of the deposited Ni NWs inside the alumina nanopores. SEM images (a) – (d) show surface views of the samples after 1μm ion milling and the images (e) – (h) show the samples cross section view.

Figure 4 displays the f_p as a function of δ_b extracted from Fig. 3. One notices that for PAA with $9 < \delta_b < 11$ nm , f_p is over 95%, peaking for 10 nm. However, an abrupt decrease of % f_p is observed outside this interval which confirms the crucial role of δ_b on electrodeposition uniformity. We can then establish that the optimized δ_b value for Ni NWs filling inside PAA membranes is (10 ± 1) nm. It is also rather striking the resemblance between the graph in Fig. 2 (c) and Fig. 3, thus showing that indeed V_e-V_i reflects distribution of the NWs.

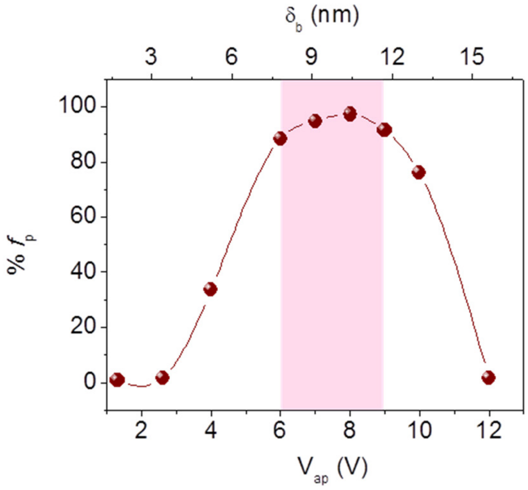

Figure 4. Dependence of f_p on V_{ap} and δ_b.

Moreover the deposition rate directly depends on the deposition current that is expected to be independent of δ_b. However, our work shows that, for a constant electrodeposition current, the deposition rate in fact depends on δ_b, as evidenced in the plot of the electrodeposition efficiency (*EE*) as a function of δ_b [Fig. 5 (a)]. *EE* was calculated using the following relation between the expected (m_t) and actual (m_a) amount of deposited metal:

$$EE = \frac{m_a}{m_t} \tag{3}$$

Since PED is a faradaic process, the metal reduction reactions are governed by Faraday's law [11] and the theoretical amount (for a current efficiency of 100%) of deposited material can be obtained from:

$$\int_0^t I dt = neN_A \frac{m_t}{M} \tag{4}$$

where I is the electrodeposition current, t the deposition time, n is the valence of the deposited ion, e the electron charge, N_A is the Avogadro constant and M the molar mass.

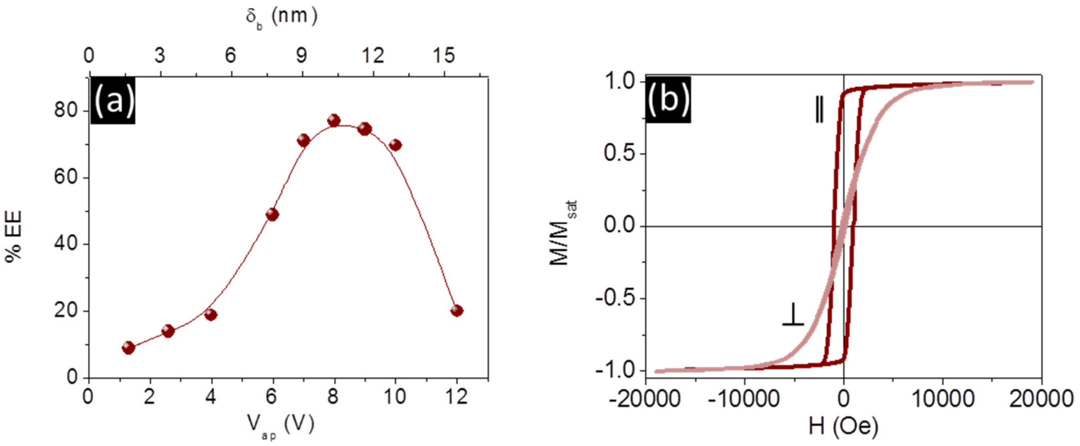

Figure 5. a) Electrodeposition efficiency as a function of V_{ap} and δ_b; b) Magnetization behavior of Ni NWs for fields transverse and parallel to the longitudinal axis of the NWs (hard and easy axis, respectively).

The actual electrodeposited mass was determined using the magnetic moment (M) of each sample obtained from SQUID measurements at room temperature. A representative normalized M versus applied magnetic field (H) curve of a Ni NW array is shown in Fig. 5 (b). Independently of their length uniformity, the M(H) measurements showed a highly anisotropic behavior characteristic of single domain-like particles with dominating shape anisotropy [21]. The coercivities in the parallel and perpendicular directions were found to be $H_c^{\parallel}$ = 1 kOe and $H_c^{\perp}$ = 100 Oe, respectively. Since saturation magnetic moment (M_{sat}) is an extensive property, we were able to extract the mass of the deposited material by simply comparing with the standard M_{sat} value of Ni NWs (M_{sat} = 50 emu/g) [25].

The *EE* shown in Fig. 5 (a) is in agreement with the f_p behavior (Fig. 4). The maximum *EE* was determined to be about 78 % for δ_b = 10 nm. Although the current efficiency in DC electrodeposition using a Watts bath is around 100% [11], the particular PED conditions used are considerable different, since our working electrode comprises an insulator oxide layer prior to the usual metallic electrode. Furthermore, the PED process is always performed above the potential for water electrolyses (1.3 V) and thus a competition with the metal deposition reaction always occurs. Nevertheless, the optimization of δ_b has provided a considerable improvement in the *EE* of PED, because the minimization of the competing side reactions was possible.

We found both the best *EE* and the f_p values (about 78% and 97%, respectively) for well-defined δ_b range of (10 ± 1) nm. However, outside this range, the *EE* and the f_p decreases abruptly, what was already expected from the electrodeposition global behavior.

Our overall results, for low δ_b, can be explained taking to account the porosity and the anodization regime for low applied potentials that lead to a broader δ_b distribution. The porosity is related with the number of branched pores (n) which is known to depend on the applied potential according to $V_\delta = {}^{1}\!/_{\sqrt{n}}\, V_S$, where V_δ is the potential to reduce the δ_b and V_S is the potential used to growth the stem pores [26]. This indicates that all the samples with $9 < \delta_b < 16$ nm have the stem pores branched in 16 dendrites, and thus only δ_b changes for each sample. However, for δ_b lower than 9 nm (i.e. 7.2 V) the number of dendrites per stem pore increases from 16 to 32, successively increasing with the decrease of δ_b. This increase in the number of the branched pores translates into an increase in the porosity. For low δ_b, the deviation from the self-ordered anodization regime for anodization potentials below 6 V ($\delta_b = 7.8$ nm) was also mentioned by Zang *et al.* [4]. Such local fluctuations in δ_b values leads to a rapid electrodeposition into the pores with smaller δ_b, to a reduced electrodeposition rate in the neighboring ones, and consequently to a non-homogeneous NWs growth [Fig. 2 (d)]. In this case, because the current flows mainly through the pores with low δ_b, an increase in the local temperature occurs, leading to an increase in the pH and consequently hydrogen evolution which inhibits NW growth [27].

On the other hand, for high δ_b, the required high voltages decrease the *EE* [as shown in Fig. 5(a)] due to the hydrogen evolution [28]. This leads to an increase in pH at the interface between the electrolyte and the deposition surface. The reaction $2H_3O^- + 2e^- = 2H_2 + 2H_2O$ then occurs, reducing metal electrodeposition. The high applied potentials and the δ_b fluctuations lead to high local current densities at the thinner regions of the barrier, and thus dielectric breakdown [15, 29]. In fact, as shown in Fig. 2 (a), the sample with $\delta_b = 16$ nm shows a sharp increase of V_{dep} followed by an abrupt decrease after two minutes of electrodeposition indicative of oxide rupture. This clearly confirms the strong influence of δ_b on the electrodeposition process. Therefore, the proper choice of δ_b results in a strong improvement of the NWs electrodeposition homogeneity and efficiency.

Another aspect which should be taken into account concerning the uniform growth of long NWs is the current density. In fact, increased uniformity can be achieved by applying relatively high constant current density pulses (70 $mAcm^{-2}$) [8]. A high current density results in high nucleation rates [13], which are followed by NWs growth, without significantly affecting structural properties (e.g., grain size around 10 nm).

The optimization of δ_b for PED in PAA can also be applied to other materials such as Fe, Co or Ni-alloys and multilayers of these materials. The optimized method lead us to fabricate highly uniform arrays of NWs which can be directly used for new applications such as plasmonic sensors and metamaterials, or dissolved PAA yielding monodisperse high NWs with promising bioapplications.

4. Conclusions

Pore filling in PAA templates was accurately controlled by varying the thickness of the alumina barrier layer (δ_b). We used δ_b values between 2 and 16 nm, and found filling rates ranging from almost 5 % to nearly 100 %, with the highest NWs filling percentage for $\delta_b = (10 \pm 1)$ nm. An increase of the electrodeposition efficiency and NW homogeneity with δ_b was also verified from 2 to 10 nm. In this range, the increase in δ_b reduces the distribution of its nominal value preventing NW growth only in the low δ_b

samples, leading to a complete and uniform pore filling. The further increase of δ_b (up to 16 nm) was followed by a decrease of the electrodeposition efficiency and the pore filling percentage, presumably due to hydrogen evolution and dielectric breakdown of the insulator layer, which were found to be inevitable due to the required high deposition voltages. A nearly 100% pores filling percentage for Ni, together with an electrodeposition efficiency around 80% was found for δ_b of 10 nm. This considerable improvement of *EE* for PED leads to the growth of NWs with several μm and a complete PAA template filling.

Acknowledgements

Work supported in part by projects NANO/NMED-SD/0140/2007 and FEDER/POCTI/n2-155/94. Funding from FCT through the Associated Laboratory-IN is acknowledged. C.T. Sousa, D.C. Leitao, and M.P. Proenca are thankful to FCT for doctoral grants SFRH/BD/38290/2007, SFRH/BPD/72359/2010 and SFRH/BD/43440/2008, respectively. A. Apolinário acknowledges the financial support under project PTDC/EQU-EQU/107990/2008. J. Ventura acknowledges financial support through FSE/POPH.

References

[1] Yao J, Liu Z, Wang Y, Sun C, Bartal G, Stacy, AM and Zhang X 2008 *Science* 321, 930.
[2] Hu W, Crouch S A, Miller D, Aryal M and Luebke J K **2010** *Nanotechnology* 21, 385301.
[3] Masuda H and Fukuda K **1995** *Science***,** 268, 1466.
[4] Zhang F, Liu X, Pan C and Zhu J **2007** *Nanotechnology***,** 18, 345302.
[5] Nielsch K, Choi J, Schwirn K, Wehrspohn R B and Gossele U **2002** *Nano Lett.* 2**,** 677.
[6] Whitney TM, Jiang JS, Searson PC and Chien CL **1993** *Science* 261, 1316.
[7] Gelves GA, Lin B, Sundadararaj U and Haber JA **2006** *Adv. Func. Mater.* 16**,** 2423.
[8] Nielsch K, Muller F, Lee A and Gosele U **2000** *Adv. Matter.* 12, 582.
[9] Cheng W, Steinhart M, Gosele U and Wehrspohn R B **2007** *J. Mater. Chem.* 17**,** 3493.
[10] Su Z and Zhou W **2008** *Adv. Mater.* 20, 3663.
[11] Schlesinger M and Paunovic M 2000 *Modern Electroplating*, Wiley Inter-Science.
[12] Razeeb K M, Rhen F M F and Roy S **2009** *J. Appl. Phys.* 105, 083922.
[13] Rashidi A M and Anadeh A **2008** S*urf. Coat. Tech.* 202, 3772.
[14] Marquardt B, Eude1 L, Gowtham M, Cho G, Jeong HJ, Châtelet M, Cojocaru CS, Kim BS and Pribat D **2008** *Nanotechnol.* 19, 405607.
[15] Jagminiene A, Valinciusb G, Riaukaite A and Jagminas **2005** *J. Crys. Growth.* 274, 622.
[16] Lee W and Kim J C **2010** *Nanotechnology* 21, 485304.
[17] Jagminas A, Cesuniene A, Vrublevsky I, Jasulaitiene V and Ragalevicius R **2010** *Electrochim. Acta* 55, 3361.
[18] Pitzschel K, Moreno J M M, Escrig J, Albrecht O, Nielsch K and Bachmann J **2009** *ACS Nano*, *3*, 3463.

[19] Leitao DC, Apolinário A, Sousa CT, Ventura J, Sousa JB, Vazquez M and Araujo JP **2011***J. Phys. Chem C***,** 115, 8567.

[20] Rasband, W S, ImageJ, U. S. National Institutes of Health, Bethesda, Maryland, USA, http://rsb.info.nih.gov/ij/, 1997-2005.

[21] Leitao D C, Sousa CT, Ventura J, Amaral JS, Carpinteiro F, Pirota KR, Vazquez M, Sousa JB and Araujo JP **2008** *J. Non-Crys. Solids*, 354**,** 5241.

[22] Tian M, Wang J, Kurtz J, Mallouk T E and Chan M H W **2003** *Nano Lett.* 3, 919.

[23] Simmons J G **1963** J. App. Phys., 34, 1795.

[24] Buschow K H J **2007** Vol. 17, Elsevier.

[25] Fung A O, Kapadia V, Pierstorff E, Ho D and Chen Y **2008** *J. Phys. Chem. C* 112, 15085.

[26] Meng G, Jung Y J, Cao A, Vajtai R and Ajayan P M **2005** *PNAS* 102, 7074.

[27] Andrew F O, Vishal K, Pierstorff E, Ho D and Chen **2007** *J. Mater. Sci.* 42, 4738.

[28] Correia A N and Machado S A S **1998** *Electrochim. Acta.* 43, 367.

[29] Gerein N J and Haber JA **2005** *J. Phys. Chem. B*, 109, 17372.